

# Surface Impedance Tomography for Antarctic Sea Ice

C. Sampson<sup>a</sup>, K. M. Golden<sup>a</sup>, A. Gully<sup>a</sup>, A. P. Worby<sup>b</sup>

<sup>a</sup>University of Utah, Department of Mathematics  
155 S 1400 E RM 233, Salt Lake City, UT, 84112-0090 USA

<sup>b</sup>Australian Antarctic Division and ACE CRC,  
University of Tasmania, Private Bag 80, Hobart, 7001, Australia

---

## Abstract

During the 2007 SIPEX expedition in pack ice off the coast of East Antarctica, we measured the electrical conductivity of sea ice via surface impedance tomography. Resistance data from classical four-probe Wenner arrays on the surfaces of ice floes were used to indirectly reconstruct the conductivity profiles with depth, involving both the horizontal and vertical components. A common problem with these reconstructions is the lack of uniqueness of the inversions, which worsens as the number of layers in the model increases. In the past, three layer inversions have been used to help avoid non-uniqueness. However, this approach assumes that the conductivity profile of sea ice does not change very much with depth. In order to investigate the conductivity profiles one needs to use more layers in the reconstruction. A reasonable starting model is a useful tool that can be used to regularize the inverse problem, allowing a reconstruction that not only matches the Wenner impedance data but the actual profile. Using measurements of brine volume fraction for 10 cm sections of ice cores taken at the Wenner array site, and various models relating brine volume fraction to conductivity, we compare the predicted conductivity profiles based on the models to the reconstructions from the tomographic measurements. We note the close agreement with the actual data for some models and the inadequacy of others. Such models could be useful in finding a reasonable starting point for regularizing inversions, and using  $n$ -layer models to reconstruct accurate conductivity profiles. Our results help to provide a rigorous basis for electromagnetic methods of obtaining sea ice thickness data, a key gauge of the impact of climate change in the polar regions.

*Keywords:* sea ice, electrical conductivity, Wenner array, surface impedance tomography

---

## 1. Introduction

The polar sea ice packs play a fundamental role in Earth's climate system, and are leading indicators of climate change (Thomas and Dieckmann, 2003; Serreze et al., 2007). They also host extensive algal and bacterial communities which sustain life in the polar oceans (Thomas and Dieckmann, 2003; Fritsen et al., 1994). Refining predictions of climate change and the future trajectory of the polar ice packs depends on accurate knowledge of their thickness distribution. Not only is this knowledge important in comparing model predictions to observed behavior, but in specifying the initial conditions necessary to study the time evolution of these nonlinear systems. Determining the thickness distribution, however, remains an elusive problem. Due to the vast extent of the polar sea ice packs, it is impractical of course to drill the millions of holes or more that would be needed to accurately assess the thickness distribution over a particular region or time period. Thus, other methods have been and are being developed, many of which use electromag-

netic techniques, such as electromagnetic induction (EMI) devices (Haas et al., 1997; Haas, 1998, 2004; Worby et al., 1999; Reid et al., 2006) mounted on ships, planes or helicopters. Electromagnetic techniques, in general, rely on some knowledge of the effective electrical properties of sea ice and how they vary with depth, temperature, salinity, ice type, etc., in the analysis of the data to obtain thickness information.

The electrical conductivity of sea ice is also closely related to its fluid transport properties. Fluid flow through sea ice mediates a broad range of processes which are important in climatological and biological studies. These include the evolution of melt ponds in the Arctic, surface flooding and snow-ice formation in the Antarctic, the evolution of salinity profiles, convection-enhanced thermal transport, CO<sub>2</sub> fluxes, and nutrient replenishment for microbial communities. In (Golden et al., 2010) we found the electrical signature of the *rule of fives* (Golden et al., 1998a, 2007; Pringle et al., 2009), where columnar sea ice is effectively impermeable for brine volume fractions

below about 5% and increasingly permeable above this threshold. Relating fluid and electrical transport properties in this way lays the foundation for electromagnetic monitoring of the above processes.

Early DC resistivity measurements of sea ice were aimed at determining ice thickness (Fujino and Suzuki, 1963; Thyssen et al., 1974; Timco, 1979). These studies employed surface soundings using 4 electrodes in either the Wenner or Schlumberger configurations. Thyssen et al. (1974) also made *in situ* measurements of sea ice resistivity using electrodes inserted into the vertical face of a pit that was dug in the unrafted ice near one of their sites. The apparent resistivity was measured perpendicular and parallel to the ice surface, and this data was analyzed further by Timco (1979). He attempted to interpret sounding results in terms of the sea ice microstructure, and it was also possible to see changes in the resistivity structure during spring warming. Nevertheless, such measurements have been somewhat unfruitful as a means of investigating either ice thickness or microstructural detail. Later measurements in the Antarctic were also reported (Buckley et al., 1986). The anisotropic nature of the resistivity of sea ice leads to measurements significantly underestimating the ice thickness (Reid et al., 2006) by a factor  $\sqrt{\rho_v^*/\rho_h^*}$ , where  $\rho_v^*$  and  $\rho_h^*$  are, respectively, the vertical and horizontal components of the bulk resistivity (Bhattacharya and Patra, 1968), with  $\sigma_v^* = 1/\rho_v^*$  and  $\sigma_h^* = 1/\rho_h^*$ , the vertical and horizontal components of the bulk conductivity. Surface measurements also lead only to an estimate of the geometric mean resistivity  $\sqrt{\rho_v^* \rho_h^*}$ .

More promising determinations of sea ice thickness have been achieved using low frequency electromagnetic induction (EMI) techniques (Haas et al., 1997; Haas, 1998, 2004; Worby et al., 1999; Reid et al., 2006). The technique relies on a time varying primary magnetic field generated by a transmitter coil. The measured secondary magnetic fields are due to the currents induced within a volume of the subsurface (i.e., the footprint) by the EMI system. The measured secondary fields at the receiver are a weighted average of the response due to all the currents within the footprint. The thickness has been found using empirical relationships (Haas, 2003), with good results for smooth ice and underestimates near ridges (Haas, 2003). However, theoretical approaches (Kovacs and Holladay, 1990; Prinsenberg et al., 2002) have also been used, where the measured secondary fields are inverted for sea ice thickness (and hopefully, the sea water conductivity and horizontal sea ice conductivity). The inversion approach assumes very accurate calibration of the EMI system. The EMI technique is adaptable to continuous measurements being made either from a helicopter or ship (Haas, 1998; Reid et al., 2006; Kovacs and Holladay, 1990; Prinsenberg et al., 2002). Theoretical modeling of electromagnetic measurements suggests a sea ice resistivity

of some 10's of  $\Omega$  m (Haas et al., 1997; Reid et al., 2006) – in broad agreement with DC resistivity determinations of  $\sqrt{\rho_v^* \rho_h^*}$ , although electromagnetic measurements as yet have been unable to provide any microstructural information. Moreover, theoretical results which accurately relate effective electrical properties of sea ice to key parameters characterizing the brine phase have been lacking.

As a step toward providing a deeper understanding of the electrical properties of sea ice, and in particular how they depend on the brine microstructure and vary with depth, we made measurements of these properties in the Antarctic. During September and October of 2007, two of us (K. M. G. and A. G.) measured the electrical conductivity of first year Antarctic pack ice as participants in the Australian Sea Ice Physics and Ecosystem Experiment (SIPEX), aboard the icebreaker *Aurora Australis*. The study area was located off the coast of East Antarctica, between 115° E and 130° E, and 64° S and 66° S. At 12 of the 15 ice stations along the cruise track of the *Aurora*, we conducted electrical soundings using a Wenner array with probes inserted into the surface of the ice over a range of spacings. The separation of the probes ranged from 5 centimeters to 5 meters. We also extracted full ice cores at each site and took temperature and salinity profiles for each core in order to obtain a brine volume profile for the ice where we measured electrical properties. Using an inversion scheme, we reconstructed information about the conductivity profile with depth. In (Golden et al., 2010) we reported on direct measurements of the vertical conductivity of the ice, and theoretical models relating sea ice electrical properties to the characteristics of the brine microstructure. We use the theoretical results here to help constrain the inversion scheme.

## 2. The bulk conductivity of sea ice

Sea ice is a complex, high contrast composite material of pure ice with brine and air inclusions. What determines the response of an ice floe in a Wenner sounding is the effective or bulk conductivity of the sea ice and its variation with depth. Predicting the effective electromagnetic properties of sea ice, such as its electrical conductivity, is a challenging theoretical problem. While pure ice and air are essentially electrical insulators, the brine phase is highly conducting. The relative volume fraction  $\phi$  of brine, the geometry of the inclusions, and in particular their connectivity, are all highly dependent on temperature (Perovich and Gow, 1996; Golden et al., 1998a, 2007; Pringle et al., 2009). The brine inclusions in general display a preferred elongation in the vertical direction, as does the brine connectivity (Golden et al., 2007; Pringle et al., 2009). The conductivity tensor of sea ice is thus anisotropic.

Let us briefly formulate the problem of finding the effective or bulk conductivity of a two phase composite material (Golden and Papanicolaou, 1983; Golden et al., 1998b; Gully et al., 2007). For these considerations we ignore the air phase in sea ice. Let the local conductivity  $\sigma(x)$  be a spatially stationary random field in  $x \in \mathbb{R}^3$ , for an appropriate probability space representing the set of realizations of the random medium. While sea ice may exhibit significant variations in microstructural properties over its entire depth, relatively thin layers such as 5 or 10 centimeters often display only small variations in these properties. It is then reasonable to assume that in typical sample sizes on this scale, the statistics describing the brine microstructure in such a region are represented by a stationary random function throughout all of  $\mathbb{R}^3$ . We assume  $\sigma(x)$  takes the value  $\sigma_1 = \sigma_b$  in the brine phase, which depends on temperature  $T$  via (Stogryn and Desargant, 1985)

$$\sigma_b = -T \exp(0.5193 + 0.08755T) \Omega^{-1} \text{ m}^{-1}, \quad (1)$$

$$T \geq -22.9^\circ \text{C}.$$

In the ice phase,  $\sigma(x)$  takes the value  $\sigma_2 = \sigma_i = 1.1 \times 10^{-8} \Omega^{-1} \text{ m}^{-1}$ , which is the value at  $T = -10^\circ \text{C}$  (Hobbs, 1974). The value in ice is effectively 0 compared to the values of  $\sigma_b$  in brine, which lie between about 3 and 7  $\Omega^{-1} \text{ m}^{-1}$ . We write  $\sigma = \sigma_1 \chi + \sigma_2 (1 - \chi)$ , where  $\chi(x)$  is the characteristic function of the brine phase, with  $\chi(x) = 1$  for  $x$  in the brine and  $\chi(x) = 0$  for  $x$  in the ice. The brine volume fraction  $\phi$  is given by  $\phi = \langle \chi \rangle$ , where  $\langle \cdot \rangle$  means an ensemble average or spatial average over all of  $\mathbb{R}^3$ , and depends on temperature  $T$  ( $^\circ \text{C}$ ) and salinity  $S$  parts per thousand (ppt) through the Frankenstein-Garner relation (Frankenstein and Garner, 1967),

$$\phi = \frac{S}{1000} \left( \frac{49.185}{|T|} + 0.532 \right). \quad (2)$$

Let  $E(x)$  and  $J(x)$  be the stationary random electric and current fields satisfying the constitutive law  $J(x) = \sigma(x)E(x)$  and the equations

$$\nabla \times E(x) = 0, \quad \nabla \cdot J(x) = 0, \quad (3)$$

with  $\langle E(x) \rangle = e_k$ , where  $e_k$  is a unit vector in the  $k^{\text{th}}$  direction for some  $k = 1, 2, 3$ . The effective conductivity tensor  $\sigma^*$  is defined by (Golden and Papanicolaou, 1983)

$$\langle J \rangle = \sigma^* \langle E \rangle. \quad (4)$$

For convenience, we focus on one diagonal coefficient  $\sigma^* = \sigma_{kk}^*$ . Due to the homogeneity of effective parameters,  $\sigma^*(\lambda\sigma_1, \lambda\sigma_2) = \lambda\sigma^*(\sigma_1, \sigma_2)$ , where  $\lambda$  is any scalar,  $\sigma^*$  depends only on the ratio  $h = \sigma_1/\sigma_2$ , and we define  $m(h) = \sigma^*/\sigma_2$ . The two main properties of  $m(h)$  are that it is analytic off  $(-\infty, 0]$  in the  $h$ -plane, and that it maps

the upper half plane to the upper half plane, so that it is an example of a Herglotz, or Stieltjes function.

An integral representation (Bergman, 1978; Milton, 1980; Golden and Papanicolaou, 1983; Golden, 1986; Milton and Golden, 1990) for  $m(h)$  which provides an important relationship between microstructural information and the effective conductivity is

$$\mathcal{F}(s) = 1 - m(h) = \int_0^1 \frac{d\mu(z)}{s - z}, \quad (5)$$

$$s = 1/(1 - h), \quad s \notin [0, 1],$$

where  $\mathcal{F}(s)$  is analytic off  $[0, 1]$ , and  $\mu$  is a positive measure on  $[0, 1]$ . Formula (5) separates the parameter  $s$  from information about the mixture geometry contained in  $\mu$ , which is a spectral measure of the operator  $\Gamma\chi$ , where  $\Gamma = \nabla(-\Delta)^{-1}\nabla$ . Statistical assumptions about the random medium (via the correlation functions) are incorporated through the moments  $\mu_n$  of  $\mu$ . For example,  $\mu_0 = \int_0^1 d\mu(z) = \langle \chi \rangle = \phi$ , the porosity. Rigorous bounds on  $\sigma^*$  can be obtained from (5) (Bergman, 1978; Milton, 1980; Golden and Papanicolaou, 1983; Golden, 1986). Comparisons of conductivity data with these bounds will be presented elsewhere.

Archie's law (Archie, 1942) is an empirical equation relating the bulk conductivity  $\sigma^*$  of a porous medium to its porosity and the conductivity  $\sigma_f$  of the fluid occupying the pore space,

$$\sigma^* = a\sigma_f\phi^m. \quad (6)$$

In this relation,  $\phi$  is the relative volume fraction of the fluid, or porosity, and  $a$  is an empirical scaling parameter often taken to be 1, which yields the correct limiting behavior as  $\phi \rightarrow 1$ . In sea ice where we expect somewhat different behavior in different volume fraction regimes, there is no particular reason for  $a$  to be taken to be 1. The exponent  $m$  depends on the geometry of the solid phase of the porous medium, such as the shapes of the grains in porous rock or sand.

The conductivity  $\sigma_b$  of brine depends on its temperature through equation (1). In studying how the vertical conductivity  $\sigma_v^*$  depends on brine volume fraction  $\phi$ , we note that the brine conductivity  $\sigma_b$  changes as a function of temperature, as does brine volume fraction via equation (2). It is then useful to consider the vertical formation factor

$$F = \frac{\sigma_v^*}{\sigma_b}, \quad (7)$$

which removes the dependence of the effective parameter on the changing conductivity of the brine itself, and depends only on the pore volume fraction and geometry. This parameter is commonly used in the analysis of other porous media such as brine-filled rocks and marine sands (Sahimi, 1995; Sen et al., 1981; Jackson et al., 1978), although the more standard definition is in terms of resis-

tivity,  $\rho_v^*/\rho_b$ . Archie's law in (6) for the vertical formation factor is then

$$F(\phi) = a\phi^m. \quad (8)$$

In (Golden et al., 2010) we used percolation theory to closely capture vertical conductivity data for Antarctic sea ice, with a critical threshold of about 5%. From a rigorous standpoint, the two approaches are inconsistent, in that Archie's law can be viewed as describing systems with connectivity all the way down to  $\phi = 0$ . It is nevertheless still useful to analyze the conductivity of sea ice using Archie's law, particularly to compare our findings with previous works (Thyssen et al., 1974; Reid et al., 2006; Ingham et al., 2008), as well as with previous work on fluid permeability (Golden et al., 2007). Moreover, Archie's law provides a formula for the conductivity below the threshold brine volume fraction, whereas percolation theory predicts a value of zero in this regime. By combining critical path analysis, relations between the electrical conductivity and fluid permeability, and statistical best fits, in (Golden et al., 2010) we found the following model for the formation factor, which also closely captures vertical conductivity data,

$$F(\phi) = 8.6\phi^{2.75}. \quad (9)$$

We will use this formula here in our inversion analysis of the Wenner array data. For comparison, we will also use  $F(\phi) = \phi^{1.9}$ , where  $a$  is forced to be 1, and the exponent comes from a statistical best fit, although it is close to the value of 2 arising from theoretical considerations. This second model underestimates the conductivity above the threshold more than (9), which provides a better approximation to percolation theory, and is discussed elsewhere.

### 3. Surface impedance tomography

#### 3.1. Formulation of the method for the Wenner array

In addition to the direct measurements of the vertical conductivity, Wenner soundings were conducted at 12 of the ice stations during SIPEX. A Wenner array consists of 4 electrodes spaced evenly apart, which are inserted into the surface of the sea ice. Current flows between the two outer electrodes C1 and C2 in Figure 2, and a potential difference is measured between the two inner electrodes P1 and P2. Resistance measurements for the Wenner electrode array were taken with a Yokogawa Electric Works (YEW) Specific Earth Resistance Tester operating at 38 Hz.

From the measured potential difference we can obtain an estimate for the apparent resistivity  $\rho_a^*$  via the following equation, where  $a$  is the separation distance (Parasnis, 1986),

$$\rho_a^* = 2\pi a \frac{\Delta V}{I} = 2\pi a R \quad (10)$$

The basic features of the Wenner soundings are as follows: (1) As the separation distance  $a$  is increased, the current penetrates deeper into the ice. (2) The apparent resistivity  $\rho_a^*$  changes for each measurement. (3) A curve of the apparent ice resistivities can be constructed from the measurements. (4) The sounding curve data can then be inverted to obtain a layered model of resistivities.

It can be shown (Bhattacharya and Patra, 1968) that for a given Wenner array spacing  $a$ , the apparent resistivity measured at the surface is:

$$\rho_a^* = \rho_1^* (1 + 4G(a) - 4G(2a)), \quad (11)$$

where

$$G(x) = 1 + 2x \int_0^\infty K(\lambda) J_0(\lambda x) d\lambda, \quad (12)$$

$J_0$  is the Bessel function of order zero and  $K(\lambda)$  is a function depending on the resistivities and thicknesses of all the layers. An example of  $K(\lambda)$  comes from a two layered earth model,

$$K(\lambda) = \frac{-k_1 e^{-2\lambda h_1}}{1 + k_1 e^{-2\lambda h_1}}, \quad k_1 = \frac{\rho_1^* - \rho_2^*}{\rho_1^* + \rho_2^*}, \quad (13)$$

where  $\rho_1^*$  and  $\rho_2^*$  are the apparent resistivities of the first and second layer, respectively,  $h_1$  is the depth of the first layer, and the second layer is a homogeneous half-space.

For our measurements the spacing value  $a$  ranged initially from .05 m to 20 m with the midpoint of the array at a fixed position. Above a 5 m spacing, however, the instrument could no longer give a reading. The lack of a reading at large  $a$  is probably because the potential difference between the receiver electrodes becomes very small over conductive sea water, and the voltage resolution limit of the meter has been reached. This behavior was observed at each ice station. The data from 5 ice stations are presented in Table 1.

We analyze our Wenner data in two ways. First, we do preliminary three layer inversions following closely the method used by Reid et al. (2006). This allows us to get an idea of the factor of anisotropy. Second, we compare the Wenner data to the conductivity models discussed above namely, Archie's law with  $a = 1$ ,  $m = 1.9$  and with  $a = 8.6$ ,  $m = 2.75$  (which is closer to percolation theory) by building an n-layer model yielding a theoretical sounding curve. We compare this to the measured curve. This comparison is useful, because we will see that for different ranges of  $\phi$  the differences between percolation theory *vs.* Archie's Law are reflected in the Wenner analysis as well.

#### 3.2. Preliminary three layer inversions

We now present the results of simple three layer inversions of the Wenner array data obtained during the SIPEX 2007 expedition. These 3-layer models will become important in the following sections and shed light



Figure 1: A Wenner electrode array along the surface of Antarctic sea ice, with the *Aurora Australis* in the background. A current  $I$  is injected through the outer electrodes C1 and C2. The potential difference  $\Delta V$  resulting from the current flow is measured at the inner electrodes P1 and P2.

$a$ (m)	$\rho_a^*$ (ohm m)				
	Station 5	Station 6	Station 8	Station 13	Station 14
0.05	62.83	7.85	4.62	5.91	5.03
0.08	60.32	9.30	5.83	7.29	6.03
0.125	113.88	11.78	8.01	10.45	6.52
0.2	113.1	15.71	10.3	11.81	8.29
0.32	114.1	20.11	12.87	11.26	10.05
0.5	71	20.42	13.19	8.64	10.68
0.8	25.13	16.08	8.65	4.12	9.7
1.25	5.5	8.64	6.28	1.34	5.97
2.0	0.94	2.58	1.52	0.53	2.34
3.2	0.2	0.8	0.2	0.42	0.92
5.0	0	0	0	0	0

Table 1: Five sets of Wenner array data.

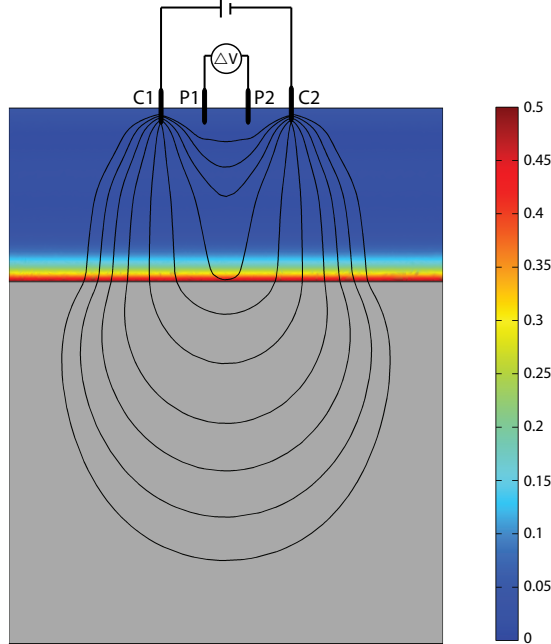


Figure 2: A Wenner array with four evenly spaced electrodes, probing a sea ice floe of thickness 0.8 m, on top of sea water. The color scale indicates the value of the vertical conductivity of the sea ice in  $(\Omega\text{m})^{-1}$ , calculated from a brine volume profile we measured in Antarctica, using  $F(\phi) = 8.6\phi^{2.75}$ . The horizontal conductivity is assumed to be 1/4 the value in the vertical direction. Comsol 3.5a was used to calculate the electric current streamlines. The conductivity of the sea water is  $4.8 (\Omega\text{m})^{-1}$ .

on the anisotropic nature of sea ice through an estimation of the factor of anisotropy. These results will allow us to relate our models for the vertical conductivity to the type of data obtained through Wenner arrays, where vertical and horizontal components of the electrical properties are mixed.

Since sea ice is horizontally isotropic when there is no preferred long term current direction (Golden and Ackley, 1981), as was the case during SIPEX, and the vertical conductivity is higher than the horizontal component, it is “transversely isotropic.” In fact, at ice station 5 we made Wenner array measurements in two orthogonal directions, and found no evidence of anisotropy in the horizontal plane. Maillet (1947) has shown that a transversely isotropic layer of actual thickness  $t_{act}$  with conductivities  $\sigma_h^*$  and  $\sigma_v^*$  yields an identical DC sounding response to an isotropic layer of thickness

$$t = \sqrt{\frac{\sigma_h^*}{\sigma_v^*}} t_{act} \quad (14)$$

and conductivity  $\sigma_m^* = \sqrt{\sigma_h^* \sigma_v^*}$ , the geometric mean of  $\sigma_h^*$  and  $\sigma_v^*$ . When we consider these relations, if we have a direct thickness measurement  $t_{act}$ , say from drilling, then we could use a sounding curve obtained from the Wenner data and invert for the thickness of the ice. Using the

actual thickness  $t_{act}$  and the inverted thickness  $t$  we can calculate the factor of anisotropy  $f = \sqrt{\sigma_h^*/\sigma_v^*}$  for the ice using

$$f = \frac{t}{t_{act}} . \quad (15)$$

The model we use to make the above calculation is a simple 3-layer model consisting of a thin, fairly conductive top layer, a thicker, less conductive middle layer and a semi-infinite, very conductive bottom layer representing the sea water.

Reid et al. (2006) have shown that typically the inversions yield a top layer which is just a few centimeters thick, which holds up under analysis of equivalent models. In this way the inverted thickness of the ice can be taken as the thickness of the second layer. The benefit of this is that the top layer is often granular and tends to be more isotropic, as the anisotropy arises from the preferred vertical orientation of the brine inclusions in columnar ice, whereas in granular ice any anisotropy is generally not so pronounced. Thus, from the model thickness of the second layer and the actual thickness obtained from drilling the ice, we can find the factor of anisotropy using  $f = t/t_a$ . We carried out the inversions using the software IP2WIN, which is used for 1-D Vertical Electrical Sounding (VES) interpretation and inversion, from the website <http://geophys.geol.msu.ru/ipi2win.htm>, V. A. Shevnin

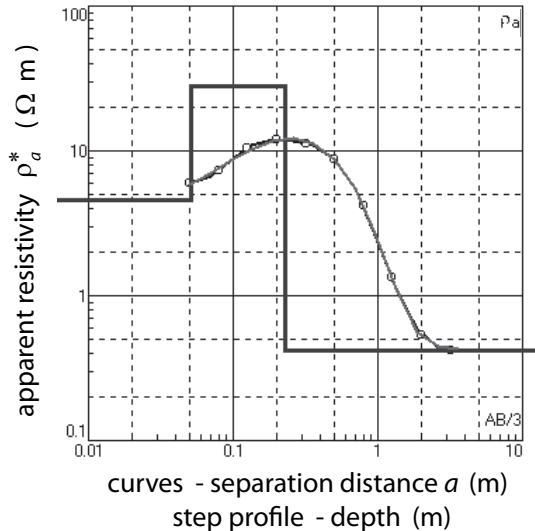


Figure 3: A typical 3-layer inversion, where the black curve connects the measured data points, the step function represents the 3-layer model, and the gray curve is the predicted sounding curve from the 3-layer model, which matches the black curve very closely. The vertical axis represents the apparent mean resistivity  $\rho_a^* = \sqrt{\rho_v^* \rho_h^*}$  while the horizontal axis represents the electrode spacing for the black and gray curves and depth for the step profile. Here the RMS error is 2.94%

and I. N. Modin, Geological Faculty, Department of Geophysics, Moscow State University.

A typical 3-layer inversion is illustrated in Figure 3, while some values for the inverted thickness and factor of anisotropy are presented in Table 2. We typically find that the factor of anisotropy  $f$  is reasonably close to 0.5, which can vary with equivalent models used. Table 2 represents some of the extreme values away from  $f = 0.5$ . A result of  $f = 0.5$  agrees with results found by Buckley et al. (1986) for undeformed first year Antarctic sea ice.

### 3.3. Comparison of Wenner data to conductivity models

For our analysis, four sets of Wenner array measurements are paired up with brine volume fraction measurements to predict a sounding curve from our models. Other stations yield good sounding curves, but do not have corresponding brine volume fraction measurements with depth. Some stations were left out of the analysis due to a large shift in the thickness of the ice over the length of the array, which renders the Wenner technique inaccurate, as uniform thickness is needed. Our general approach is outlined here:

- First we plot the measured apparent resistivity  $\rho_a^*$  vs. the spacing  $a$ .
- We then perform a simple 3-layer inversion to obtain the factor of anisotropy  $f$  and estimate the thickness and resistivity of the first layer.
- Using the factor of anisotropy we relate our models for vertical conductivity as a function of brine volume fraction  $\phi$  to the mean resistivity of the sea ice

$\rho_m^*$ . We also relate the thickness of directly measured layers to the thicknesses of layers which would yield an identical sounding curve ( $t = ft_a$ ) using the mean resistivity.

- Using our estimate of the thickness and resistivity of the first layer from the 3-layer inversion, and the thicknesses of all subsequent layers calculated from our models and  $f$ , we build an  $n$ -layer model of the resistivity of sea ice with depth (step function).
- We then compare the predicted (gray) sounding curves from these models to the measured (black) curves which connect the data points.

Given that our theoretical models reasonably represent the conductivity of sea ice, if we have measurements of the brine volume fraction  $\phi$  and the conductivity of the brine  $\sigma_b$  for different depths of the ice, we should be able to predict an  $n$ -layer model which fits a measured Wenner sounding curve. However, we must take the anisotropy of the ice into account. Here we present a general method for making this kind of prediction using our Archie's law analysis. Here  $n$  is the number of sections of an ice core for which we have measurements. Most inversion schemes for Wenner sounding data take resistivity as an input, thus we can obtain a model using  $\rho_v^* = (\sigma_v^*)^{-1} = (a\sigma_b\phi^m)^{-1}$ .

Since Wenner arrays do not resolve anisotropy, we must account for this to predict an accurate sounding curve. As mentioned before we can relate the horizontal and vertical conductivities to an equivalent isotropic conductivity through their geometric mean,  $\sigma_m^* = \sqrt{\sigma_h^* \sigma_v^*}$  and the factor of anisotropy  $f = \sqrt{\sigma_h^* / \sigma_v^*}$ . Also, as stated before, sea

Ice Station	$t$ (cm)	$t_{act}$ (cm)	$f = t/t_a$	$h_1$ (cm)
5	27.7	69	0.40	2.8
6	25.4	37	0.69	9
13	17.6	41	0.43	5.1
14	48.7	86	0.57	10

Table 2: The inverted thickness ( $t$ ), actual thickness ( $t_{act}$ ), factor of anisotropy  $f$ , and height of the first layer  $h_1$  for the Wenner measurements at four different ice stations.

ice is usually transversely isotropic. In this case (Maillet, 1947) a transversely isotropic layer with thickness  $t_{act}$  and conductivities  $\sigma_h^*$  and  $\sigma_v^*$  yields an identical DC sounding response to an isotropic layer of thickness  $t = \sqrt{\sigma_h^*/\sigma_v^*} t_a$  and conductivity  $\sigma_m = \sqrt{\sigma_h^*\sigma_v^*}$ . We mention that a much more detailed analysis of anisotropy and its effect on resistance measurements in sea ice has been done by Jones et al. (2010).

If values for  $a$  and  $m$  are determined for the vertical conductivity in Archie’s law, we can then find the equivalent isotropic resistivity  $\rho_m^*$  using the factor of anisotropy since  $f \rho_m^* = f \frac{1}{\sigma_m^*} = \frac{1}{\sigma_v^*} = \rho_v^*$ . Thus,

$$\rho_m^* = \frac{\rho_v^*}{f} = \frac{1}{f \sigma_v^*} = \frac{1}{f a \sigma_b \phi^m}. \quad (16)$$

If we have measurements for  $\phi$ ,  $\sigma_b$ , and  $f$  for a given layer, we can find the mean resistivity that would fit the Wenner sounding curve, and then we can build an  $n$ -layer model. However, finding a factor of anisotropy for each measured section is difficult. Instead we find a factor of anisotropy for the entire sea ice sheet using a simple 3-layered model inversion and the relation  $f = t_{act}/t$ , where  $t$  is the inverted thickness from the model.

From here we can build a profile of the mean resistivities at different depths given the brine volume fraction using (16). We can also calculate the apparent thickness of the layer at that depth using the known measured thickness of a layer for a given brine volume fraction and the factor of anisotropy with  $t = f t_{act}$ . It is important to note that the first layer of the inversion comes from granular ice. We allow the 3-layer inversion to predict its resistivity and thickness because it should be correct for an isotropic medium. If one does not do this, the resistivity is typically overestimated.

An overview of the  $n$ -layer inversion scheme is as follows:

1. Run a 3-layer inversion to find  $f$  and estimate the thickness and resistivity of the first layer.
2. Compute  $\rho_m^*$  for the subsequent layers using (16).
3. Compute the thickness the Wenner array “sees” for each layer with  $t = f t_{act}$ .
4. Compare the predicted sounding curve with the observed data.

Table 3 shows the results of these calculations for one of the measured sites, while Figure 4 illustrates the calculated model.

We present three separate soundings, each from different ice stations, as well as predicted sounding curves from Archie’s law with  $a = 1$  and  $m = 1.9$ , and with  $a = 8.6$  and  $m = 2.75$ . In the first case we see a similar departure from Archie’s law as mentioned in the previous section. That is, when we have higher brine volume fractions ( $\phi > 8\%$ ), Archie’s law with  $a = 1$  tends to underestimate the conductivity and thus overestimate the resistivity. For lower brine volume fractions we see the predicted curve significantly underestimate the measured sounding curve. When using  $a = 8.6$ , however, we see a predicted curve which tends to be much closer to the actual sounding curve determined from the measurements in both cases.

In Figure 4, we show the results from station 13 where the brine volume fraction ranged from  $\phi = 0.09$  to 0.22, all above the possible percolation threshold. In this case we would expect that when  $a = 1$  and  $m = 1.9$ , we should underestimate the conductivity since we are above the percolation threshold, or overestimate the resistivity. This case is shown on the left where we do in fact see overestimation. When we apply Archie’s law with  $a = 8.6$  and  $m = 2.75$ , we do not see the same overestimation and the overall shape of the predicted curve matches more closely that of the data, implying that a percolation approach may better represent the actual vertical conductivity.

In Figure 5, we show the results from station 5 where the brine volume fraction ranged from  $\phi = 0.04$  to 0.07, all below the possible percolation threshold. In this case, we should expect that when  $a = 1$  and  $m = 1.9$  we would see an overestimation of the conductivity and thus an underestimation of the resistivity. In fact, in this case we do see an underestimation of the resistivity as shown on the left in Figure 5. When we apply Archie’s law with  $a = 8.6$  and  $m = 2.75$  we see a much better fit.

In Figure 6, we show the results from station 6 where the brine volume fraction ranged from  $\phi = 0.07$  to 0.22. For this we would expect much the same behavior as for station 13 with  $a = 1$  and  $m = 1.9$  with overestimation of the resistivity due to the range of brine volume fractions. However, we see a large underestimation. This can be

Core Section (m)	$\phi$	$l$ (m)	$f \cdot l$ (m)	$\rho_m^*$ ( $\Omega\text{m}$ )
0-0.05	0.14	0.05	*	4.53
0.05-0.1	0.14	0.05	0.0215	13.2
0.1-0.2	0.09	0.1	0.43	49
0.2-0.3	0.11	0.1	0.43	32
0.3-0.41	0.19	0.1	0.47	9.2

Table 3: A six layer model, with the 6th layer being the ocean, where ice resistivity and layer thickness are calculated from brine volume fraction measurements using the model  $F(\phi) = 8.6\phi^{2.75}$  to calculate the mean resistivities as discussed in this section with  $f = 0.43$ . These measurements come from station 13 and are shown in the left of Figure 4. \* The thickness of the first layer is determined by the preliminary three layer inversion.

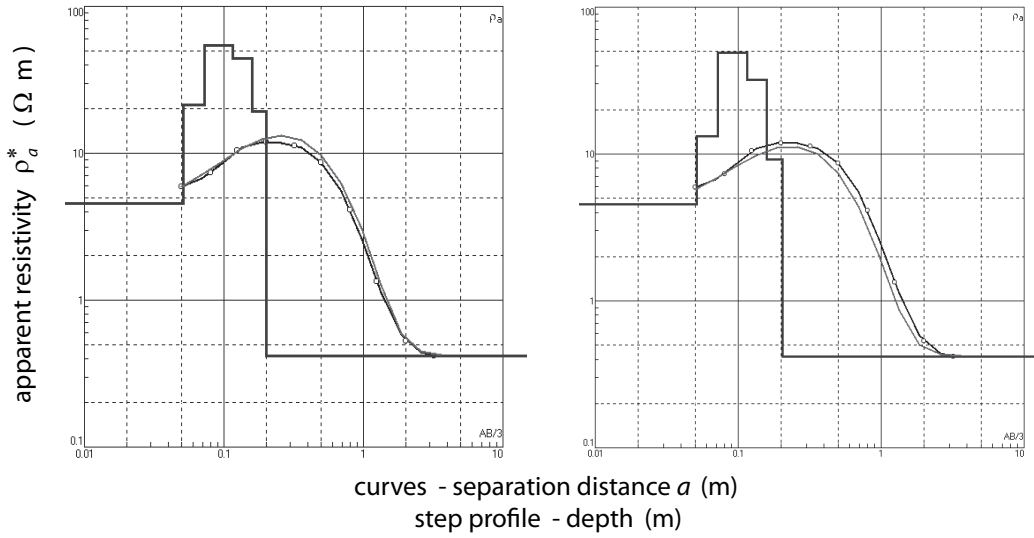


Figure 4: Ice station 13. Left: predicted curve with  $a = 1$  and  $m = 1.9$  and actual measured curve showing overestimation in the higher brine volume fraction range. Right: predicted curve with  $a = 8.6$  and  $m = 2.75$  showing close agreement with a slight underestimation.

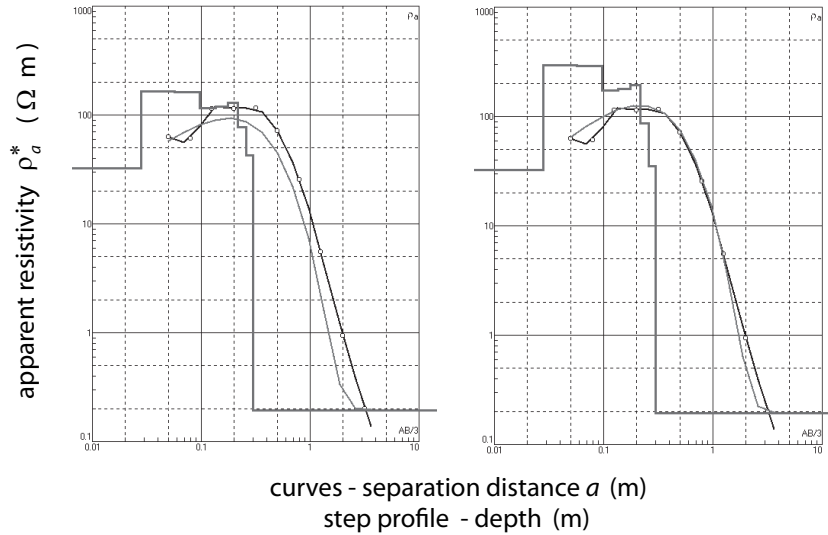


Figure 5: Ice station 5. Left: predicted curve with  $a = 1$  and  $m = 1.9$  and actual measured curve showing underestimation in the lower brine volume fraction range. Right: predicted curve with  $a = 8.6$  and  $m = 2.75$ , showing closer agreement with the measured curve.

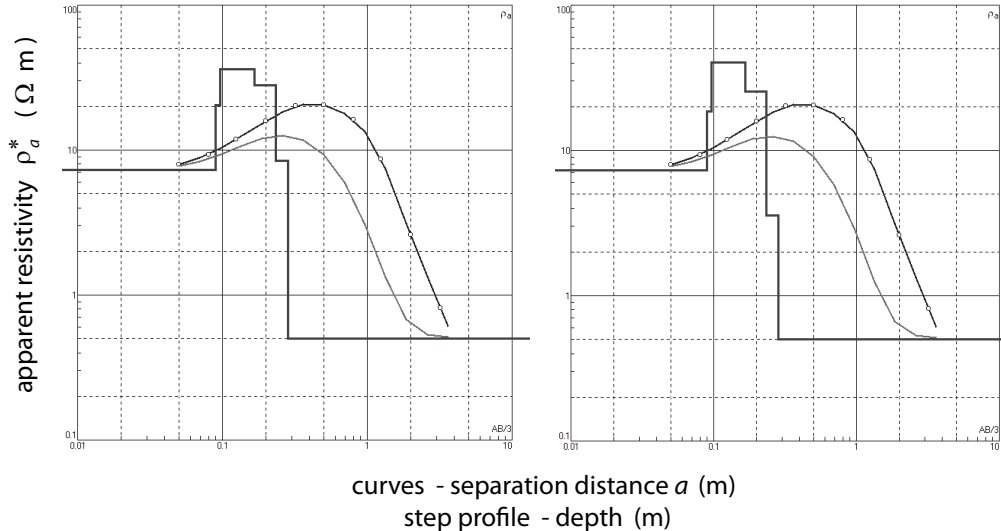


Figure 6: Ice station 6. Left: predicted curve with  $a = 1$  and  $m = 1.9$  and actual measured curve showing large underestimation in resistivities probably due to the microstructure of the ice. Right: predicted curve with  $a = 8.6$  and  $m = 2.75$  showing slightly closer agreement. The underestimation may be a result of granular ice.

understood since the conductivity values for this station are some of the highest values of the conductivity for given brine volume fractions. Thus, the associated resistivities are the lowest, which would give a large underestimation of the sounding curve. When  $a = 8.6$  and  $m = 2.75$ , we do obtain slightly higher values which put us closer to the actual curve. However, we still have an underestimation, which may be the result of granular ice where anisotropy is not as pronounced.

This method for predicting a sounding curve works well provided that the appropriate value of  $m$  is used in Archie's Law. The best results are obtained when the value of  $m$  used correlates most closely with percolation theory. The above comparison is useful as it allows us to compare our models from our direct measurements to a different data set. The fact that we see the same behavior as in the previous sections reinforces our conclusions.

In the previous sections we have used various models derived from direct measurements of vertical conductivity (Golden et al., 2010) and brine volume fraction to construct a prediction of what a Wenner sounding curve should look like at a given site. The close agreement of the predicted curves with actual soundings suggests that these theoretical curves could serve as a regularization model to aid in the construction of an  $n$ -layer resistivity profile of sea ice that represents the actual conditions.

Using the predicted model given by  $F = 8.56\phi^{2.75}$  to regularize the inversion problem, by least squares methods, we have constructed a 6-layer vertical resistivity profile for Ice Station 13. In the figure the 6th layer is the ocean which is not depicted. In this particular case we fix the total thickness of the ice as it is known from a

core sample. In a case where the actual thickness was not known an estimate can be made using the factor of anisotropy and the thickness given from the 3-layer inversion as discussed in the previous sections. Upon completion of the inversion, the vertical resistivity of each layer can be recovered by multiplying its apparent resistivity  $\rho_a$  by the factor of anisotropy  $f$ . The correct thickness of the layer can be obtained by dividing the inverted height ( $h$ ) by  $f$ . Once this is done the actual values can be plotted.

We compare the predicted model with the inverted model in Figure 7. It is apparent from the figure that the predicted and inverted profiles have similar structure suggesting a good estimate by the model. The main difference between the predicted (dashed) and inverted (solid) profiles is higher resistivity given by the inversion. This can be related back to Figure 4, as the model shown on the left slightly underestimates  $\rho_a$  for Station 13.

The 6-layer inversion in Figure 7 illustrates the subtle changes in resistivity of ice which go unnoticed in standard 3-layer models. Understanding how the resistivity changes with depth at a higher resolution may lead to more accurate models in mounted EM sounding techniques such as shipborne or airborne EM devices which currently model sea ice using only 3-layers.

It should be noted that we had available a detailed brine volume and temperature profile to use with our model. However, in principle one could use a temperature profile to estimate both brine volume fraction and brine conductivity with depth which can then be used to generate a regularization model. To illustrate the usefulness of even a less accurate, but still reasonable, regularization model in producing a realistic inverted profile, we introduce a

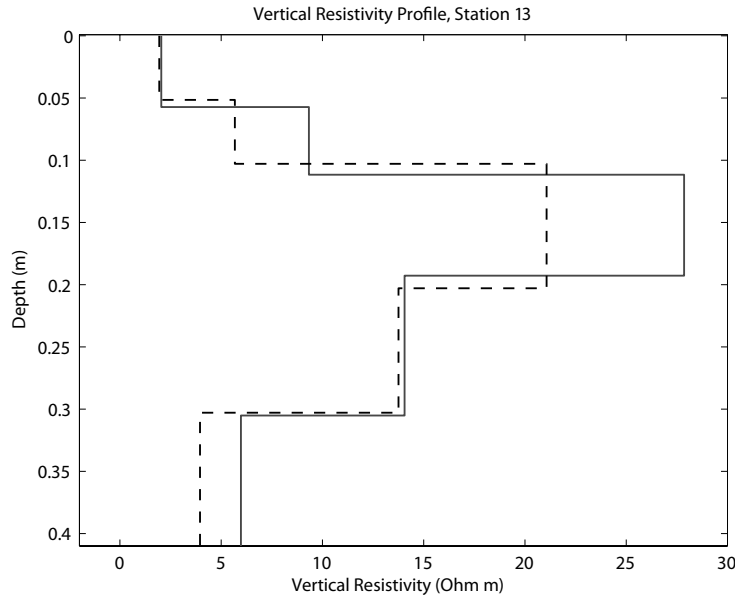


Figure 7: The the predicted (dashed) and inverted (solid) vertical resistivity profile for a 6-layer inversion of station 13 with depth. The x-axis is the resistivity while the y-axis is positively directed downward showing depth. The similar structure between the two suggests the predicted model is a good estimate

10 percent random error into the predicted model and repeat our inversion scheme using this less accurate model for regularization then compare this to the inversion result from the original predicted model in Figure 8. It can be seen from Figure 8 that the result, while not exactly the same, is not very different from that using a more accurate regularization model and shares the same overall distribution of resistivities. This is in contrast to the result obtained when not using a reasonable regularization model, i.e., a model not based on the actual properties of the ice, which we illustrate in Figure 9. The result in Figure 9 was obtained by dividing the middle layer from a simple 3-layer inversion into 4 equal pieces in both depth and resistivity while leaving the top layer and bottom layer alone, creating a hap-hazard 6-layer model to be used for regularization. We then invert using this model and compare the result to that when using the best predicted model. As can be seen in Figure 9 the results of the two inversions are completely different, yet both will produce a forward model which fits the Wenner sounding curve well. In this way it can be seen how important it is to have a reasonable regularization model to prevent extraneous solutions which do not accurately represent the sea ice.

#### 4. Conclusions

We have made indirect measurements of the electrical conductivity of Antarctic sea ice. We used Wenner array soundings to measure the apparent conductivity as

a function of separation, yielding information about the conductivity profile with depth. We developed an  $n$ -layer inversion scheme to reconstruct the profiles from the Wenner array data, which relies on a regularization technique based on conductivity models for sea ice. Our work helps to provide a rigorous basis for the interpretation of thickness soundings, but also yields information about the conductivity of sea ice with depth. Such information, when combined with other work relating fluid and electrical transport properties, helps lay the groundwork for monitoring fluid processes in sea ice which are important in climate studies.

**Acknowledgments:** We are very grateful for the support provided by the Division of Mathematical Sciences and the Arctic Natural Sciences Program at the US National Science Foundation (NSF). Adam Gully was supported by the NSF Research Experiences for Undergraduates (REU) Program and an NSF VIGRE graduate fellowship, and Christian Sampson was supported by the NSF REU Program. We thank Joyce Lin for providing Figure 2 illustrating the electric current streamlines for the Wenner array. We also thank the Australian Antarctic Division and the crew of the *Aurora Australis* for their help and support during the SIPEX Antarctic expedition.

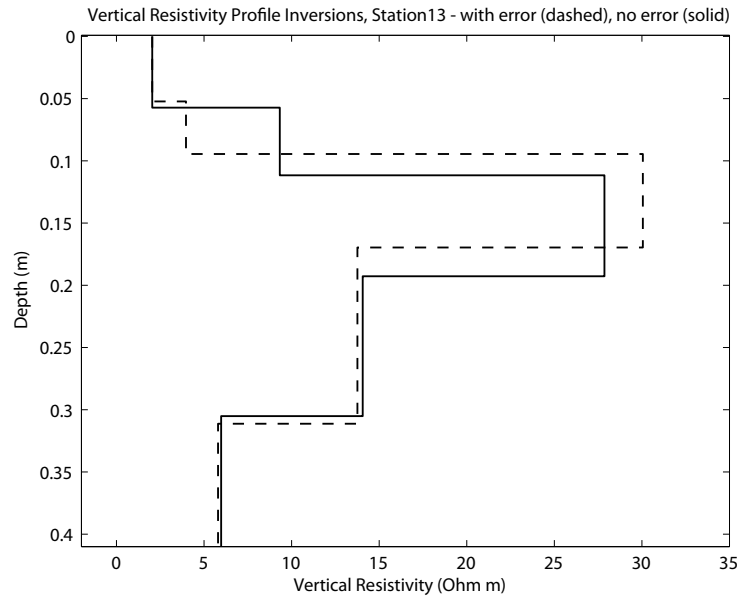


Figure 8: Inverted vertical resistivity profiles from the predicted model with (dashed) and without (solid) an introduced 10 percent random error in the regularization model. From this figure the use of a regularization model in preserving the shape of a profile is illustrated.

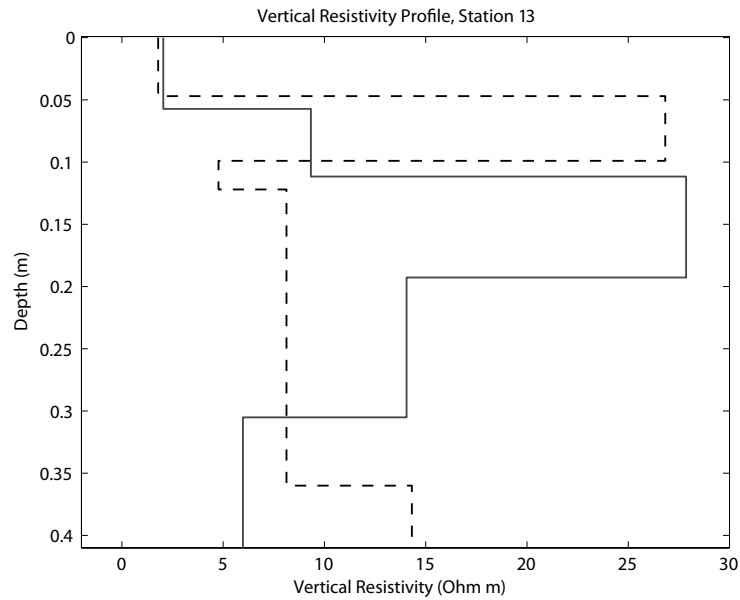


Figure 9: Inverted vertical resistivity profiles with regularization (solid) and without (dashed). It can be seen that while both profiles produce sounding curves which match the sounding data their overall structure is quite different.

## References

- Archie, G.E., 1942. The electrical resistivity log as an aid in determining some reservoir characteristics. *Trans. Am. Inst. Min. Metal. Petrol. Eng.* 146, 54–64.
- Bergman, D.J., 1978. The dielectric constant of a composite material – A problem in classical physics. *Phys. Rep. C* 43, 377–407.
- Bhattacharya, P.K., Patra, H.P., 1968. *Direct current geoelectric sounding; principles and interpretation.* Elsevier Publishing, Amsterdam.
- Buckley, R.G., Staines, M.P., Robinson, W.H., 1986. In situ measurements of the resistivity of Antarctic sea ice. *Cold Reg. Sci. Technol.* 12, 285–290.
- Frankenstein, G., Garner, R., 1967. Equations for determining the brine volume of sea ice from  $-0.5^\circ$  to  $-22.9^\circ$  C. *J. Glaciol.* 6, 943–944.
- Fritsen, C.H., Lytle, V.I., Ackley, S.F., Sullivan, C.W., 1994. Autumn bloom of Antarctic pack-ice algae. *Science* 266, 782–784.
- Fujino, K., Suzuki, Y., 1963. An attempt to estimate the thickness of sea ice by electrical resistivity method II. *Low Temp. Sci.* A21, 151–157.
- Golden, K., 1986. Bounds on the complex permittivity of a multi-component material. *J. Mech. Phys. Solids* 34, 333–358.
- Golden, K., Papanicolaou, G., 1983. Bounds for effective parameters of heterogeneous media by analytic continuation. *Comm. Math. Phys.* 90, 473–491.
- Golden, K.M., Ackley, S.F., 1981. Modeling of anisotropic electromagnetic reflection from sea ice. *J. Geophys. Res. (Oceans)* 86, 8107–8116.
- Golden, K.M., Ackley, S.F., Lytle, V.I., 1998a. The percolation phase transition in sea ice. *Science* 282, 2238–2241.
- Golden, K.M., Cheney, M., Ding, K.H., Fung, A.K., Grenfell, T.C., Isaacson, D., Kong, J.A., Nghiem, S.V., Sylvester, J., Winebrenner, D.P., 1998b. Forward electromagnetic scattering models for sea ice. *IEEE Trans. Geosci. Rem. Sens.* 36, 1655–1674.
- Golden, K.M., Eicken, H., Gully, A., Ingham, M., Jones, K.A., Lin, J., Reid, J., Sampson, C., Worby, A.P., 2010. Critical behavior of electrical transport in sea ice. In preparation.
- Golden, K.M., Eicken, H., Heaton, A.L., Miner, J., Pringle, D., Zhu, J., 2007. Thermal evolution of permeability and microstructure in sea ice. *Geophys. Res. Lett.* 34, L16501 (6 pages and issue cover), doi:10.1029/2007GL030447.
- Gully, A., Backstrom, L.G.E., Eicken, H., Golden, K.M., 2007. Complex bounds and microstructural recovery from measurements of sea ice permittivity. *Physica B* 394, 357–362.
- Haas, C., 1998. Evaluation of ship-based electromagnetic-inductive thickness measurements of summer sea-ice in the Bellingshausen and Amundsen Seas, Antarctica. *Cold Reg. Sci. Tech.* 27, 1–16.
- Haas, C., 2003. Dynamics versus thermodynamics: The sea ice thickness distribution, in: Thomas, D.N., Dieckmann, G.S. (Eds.), *Sea Ice: An Introduction to its Physics, Chemistry, Biology and Geology.* Blackwell, Oxford, pp. 82–111.
- Haas, C., 2004. Late-summer sea ice thickness variability in the Arctic Transpolar Drift 1991–2001 derived from ground-based electromagnetic sounding. *Geophys. Res. Lett.* 31, L09402, doi:10.1029/2007GL030447.
- Haas, C., Gerland, S., Eicken, H., Miller, H., 1997. Comparison of sea-ice thickness measurements under summer and winter conditions in the Arctic using a small electromagnetic induction device. *Geophysics* 62, 749–757.
- Hobbs, P.V., 1974. *Ice Physics.* Clarendon Press, Oxford.
- Ingham, M., Pringle, D.J., Eicken, H., 2008. Cross-borehole resistivity tomography of sea ice. *Cold Reg. Sci. Technol.* 52, 263–277, 10.1016/j.coldregions.2007.05.002.
- Jackson, P.D., Smith, D.T., Stanford, P.N., 1978. Resistivity-porosity-particle shape relationships for marine sands. *Geophysics* 43, 1250–1268.
- Jones, K.A., Ingham, M., Pringle, D.J., Eicken, H., 2010. Temporal variations in sea ice resistivity: resolving anisotropic microstructure through cross-borehole dc resistivity tomography. *J. Geophys. Res.*, in press.
- Kovacs, A., Holladay, J.S., 1990. Sea ice thickness measurement using a small airborne electromagnetic sounding system. *Geophysics* 55, 1327–1337.
- Maillet, R., 1947. The fundamental equations of the electrical prospecting. *Geophysics* 12(4), 529–556.
- Milton, G.W., 1980. Bounds on the complex dielectric constant of a composite material. *Appl. Phys. Lett.* 37, 300–302.
- Milton, G.W., Golden, K., 1990. Representations for the conductivity functions of multicomponent composites. *Comm. Pure. Appl. Math.* 43, 647–671.
- Parasnis, D.S., 1986. *Principles of Applied Geophysics, Fourth Edition.* Chapman and Hall, New York.
- Perovich, D.K., Gow, A.J., 1996. A quantitative description of sea ice inclusions. *J. Geophys. Res.* 101, 18,327–18,343.
- Pringle, D.J., Miner, J.E., Eicken, H., Golden, K.M., 2009. Pore-space percolation in sea ice single crystals. *J. Geophys. Res. (Oceans)* 114 (C12017).
- Prinsenber, S.J., Holladay, S., Lee, J., 2002. Measuring ice thickness with EISFlow, a fixed-mounted helicopter electromagnetic-laser system, in: Chung, J.S., Sayed, M., Kashiwagi, M., Setoguchi, T., Hong, S.W. (Eds.), *The Proceedings of the Twelfth International Conference on Offshore and Polar Engineering, Kitakyushu, Japan.* International Society of Offshore and Polar Engineers, Cupertino, CA. volume 1, pp. 737–740.
- Reid, J.E., Pfaffing, A., Worby, A.P., Bishop, J.R., 2006. In situ measurements of the direct-current conductivity of Antarctic sea ice: Implications for airborne electromagnetic sounding of sea-ice thickness. *Ann. Glaciol.* 44, 217–223.
- Sahimi, M., 1995. *Flow and Transport in Porous Media and Fractured Rock.* VCH, Weinheim.
- Sen, P.N., Scala, C., Cohen, M.H., 1981. A self-similar model for sedimentary rocks with application to the dielectric constant of fused glass beads. *Geophysics* 46, 781–795.
- Serreze, M.C., Holland, M.M., Stroeve, J., 2007. Perspectives on the Arctic’s shrinking sea-ice cover. *Science* 315, 1533–1536.
- Stogryn, A., Desargant, G.J., 1985. The dielectric properties of brine in sea ice at microwave frequencies. *IEEE Trans. Antennas Propagat.* AP-33, 523–532.
- Thomas, D.N., Dieckmann, G.S. (Eds.), 2003. *Sea Ice: An Introduction to its Physics, Chemistry, Biology and Geology.* Blackwell, Oxford.
- Thyssen, F., Kohnen, H., Cowan, M.V., Timco, G.W., 1974. DC resistivity measurements on the sea ice near pond inlet. *Polarforschung* 44, 117–126.
- Timco, G.W., 1979. An analysis of the in-situ resistivity of sea ice in terms of its microstructure. *J. Glaciol.* 22, 461–471.
- Worby, A.P., Griffin, P.W., Lytle, V.I., Massom, R.A., 1999. On the use of electromagnetic induction sounding to determine winter and spring sea ice thickness in the Antarctic. *Cold Reg. Sci. Tech.* 29, 49–58.